Impact of sandpaper grit size on drag reduction and plastron stability of super-hydrophobic surface in turbulent flows *♥*

Shabnam Mohammadshahi 💿 ; Daniel O'Coin 💿 ; Hangjian Ling 🗷 💿



Physics of Fluids 36, 025139 (2024) https://doi.org/10.1063/5.0187081





CrossMark

International Journal of Fluid Engineering 国际流体工程

No Article Processing Charges (APCs)

Diamond Open Access



Impact of sandpaper grit size on drag reduction and plastron stability of super-hydrophobic surface in turbulent flows

Cite as: Phys. Fluids **36**, 025139 (2024); doi: 10.1063/5.0187081 Submitted: 10 November 2023 · Accepted: 24 January 2024 · Published Online: 20 February 2024







Shabnam Mohammadshahi, 🕞 Daniel O'Coin, 🕞 and Hangjian Ling 🗈 🕞





AFFILIATIONS

Department of Mechanical Engineering, University of Massachusetts Dartmouth, Dartmouth, Massachusetts 02747, USA

a) Author to whom correspondence should be addressed: hling1@umassd.edu

ABSTRACT

In this work, we experimentally investigated the impact of surface roughness on drag reduction as well as the plastron stability of superhydrophobic surfaces (SHSs) in turbulent flows. A series of SHSs were fabricated by spraying hydrophobic nanoparticles on sandpapers. By changing the grit size of sandpapers from 240 to 1500, the root mean square roughness height (k_{rms}) of the SHSs varied from 4 to 14 μ m. The experiments were performed in a turbulent channel flow facility, where the mean flow speed (U_m) varied from 0.5 to 4.4 m/s, and the Reynolds number (Re_m) based on U_m and channel height changed from 3400 to 26 400. The drag reduction by SHSs was measured based on pressure drops in the fully developed flow region. The plastron status and gas fraction (φ_g) were simultaneously monitored by reflected-light microscopy. Our results showed a strong correlation between drag reduction and $k_{rms}^+=k_{rms}/\delta_{\nu}$, where δ_{ν} is the viscous length scale. For $k_{rms}^+ < 1$, drag reduction was independent of k_{rms}^+ . A maximum 47% drag reduction was observed. For $1 < k_{rms}^+ < 2$, less drag reduction was observed due to the roughness effect. And for $k_{rms}^+ > 2$, the SHSs caused an increase in drag. Furthermore, we found that surface roughness influenced the trend of plastron depletion in turbulent flows. As increasing Re_m , φ_g reduced gradually for SHSs with large k_{rms} , but reduced rapidly and maintained as a constant for SHSs with small k_{rms} . Finally, we found that as increasing Re_m , the slip length of SHS reduced, although φ_g was nearly a constant.

Published under an exclusive license by AIP Publishing. https://doi.org/10.1063/5.0187081

I. INTRODUCTION

Superhydrophobic surfaces (SHSs) are widespread in nature.^{1,2} They have attracted tremendous attention due to their wide range of potential applications in diverse fields, including engineering and various scientific disciplines such as hydrodynamic drag reduction,³ self-cleaning,^{6,7} anti-biofouling,^{8–10} and enhancing heat and mass transfer.^{11–13} Among these applications, drag reduction stands out as a compelling factor emphasized in almost every publication on SHS, owing to its global-scale impact on conserving energy and protecting the environment.¹⁴ The reason that SHSs can reduce drag is mainly because SHSs trap a thin layer of gas (or plastron) between the surface textures when contacting with liquid, promoting the so-called Cassie-Baxter state. Due to the lower viscosity of the gas compared to the liquid, the SHSs support an effective slip boundary, characterized by a slip length b, and reduce the near-wall velocity gradients. For a smooth surface, b is typically on the order of a few nanometers. However, for a SHS with microtextures, b can reach to the order of a few hundred micrometers. 15 Drag reduction is achieved when b is comparable to

the characterized length scale of the flow, e.g., channel height for laminar channel flows, 3,16,17 viscosity length scale δ_{ν} for turbulent boundary layers, 18 and diameter of the object for external flows over objects. 19,20 In the past two decades, the drag-reducing property of SHS in turbulent flows has been extensively studied through a combination of numerical, experimental, and theoretical approaches. It is generally understood that large drag reduction (up to 90%²¹) can be generated when the gas layer is maintained on the SHS and when $b^+ = b/\delta_v > 1$ (Ref. 18). Researchers have also shown the degradation of drag reduction due to various factors such as surface roughness, 4,22,23 spanwise slip, 24,25 pressure, 4 curved or depining of the gasliquid interface, 26,27 gas dissolution in undersaturated liquid, 28,29 and surfactant. 30,31 Furthermore, researchers frequently reported that by increasing the Reynolds number, the gas on SHS was removed due to turbulence³² leading to a failure of drag reduction. To address the issue of unstable gas in turbulent flows, a number of passive and active techniques have been developed, including the modifications of surface texture by using nano-scale roughness^{33,34} or reentrant geometry,³⁵

and gas replenishment based on gas injection from an external source 37,38 (e.g., through a porous material) or *in situ* gas generation 39,40 (e.g., by decomposition of water with electric current).

Despite extensive studies in the past, the impact of surface roughness on the drag-reducing properties of SHS in turbulent flows has not been fully investigated. SHSs with randomly roughed textures are produced inevitably on large-scale SHSs fabricated by methods such as chemical etching,⁴¹ sandblasting,^{42–44} and sprayed coating.⁴ The surface roughness can be partially characterized by the root mean square (rms) value of roughness height denoted as k_{rms} . SHS with different values of k_{rms} could be produced by varying the size of spraying particles, the grit size of blasting media, and the duration of chemical etching. Understanding the effect of k_{rms} on turbulent drag reduction could provide important guidelines for the fabrication and implementation of SHSs in large-scale applications, such as marine vessels. Although SHSs with an identical texture height and minimal surface roughness can be produced by techniques such as photolithography or laser texturing, these techniques may not be economically feasible for large-scale applications. The main aim of this paper is to systemically vary the surface roughness of SHS and investigate its impact on the drag reduction of SHS in turbulent flows.

Early experimental and numerical studies have provided valuable insights into the effect of surface roughness on the drag-reducing performance of SHS in turbulent flows. These early experimental studies4,21,22,45-47 are summarized in Table I, which lists the SHS fabrication techniques, surface roughness height, drag reduction measurement techniques, and amount of drag reduction. A common observation in these studies was that the amount of drag reduction reduces as increasing k_{rms} . Several works also showed that the SHS transitioned from the drag reduction regime to the drag increase regime when $k_{rms}^{+} = k_{rms}/\delta_{v}$ was larger than a critical value close to 1.^{22,45} Furthermore, Gose et al.²¹ found that the drag reduction of different SHS had a strong correlation with the product of k_{rms}^{+} and contact angle hysteresis. Rajappan et al.48 found that the large lateral spacing between roughness peaks, in conjunction with a small root mean square roughness is crucial for turbulent drag reduction. A few numerical studies also showed less drag reduction by SHS due to the effect of surface roughness.^{23,49} For example, Seo and Mani⁴⁶ showed that the slip length on SHS with randomly distributed textures is 30% less than that for regular textures of the same size.

Understanding the plastron stability in turbulent flows is also crucial since the drag-reducing capability of SHS mainly relies on the presence of the gas layer. However, the impact of surface roughness on the plastron stability has received very little attention. A few numerical studies $^{26,49-53}$ examined the wall pressure fluctuation, p_w , applied on SHSs under turbulent flows and the resulting interface deformation. The simulations show that due to large p_w , an initially flat interface is curved, penetrates into the microcavities, and finally detaches from the tip of roughness. Large p_w can be caused by three mechanisms: (i) the stagnation of flow at the leading edges of surface textures,⁵⁰ (ii) the flow-induced capillary wave, ⁵² and (iii) the intermittent turbu-Empirical models of p_w corresponding to each mechanism have also been proposed. Moreover, using direct numerical simulations (DNS), Ma et al. 53 showed that surface roughness on SHS causes higher p_w . Several experimental works have qualitatively examined the state of the gas layer on the SHS in turbulent flows. For example, by imaging the SHS at total internal reflection angles, several researchfound that the gas layer diminishes with increasing Reynolds number (Re). Using digital holography, Ling et al.4 measured the size distribution of the entrained gas bubbles and found an increase in gas depletion rate with increasing Re. Using bright-field microscopy, Reholon and Ghaemi⁴⁵ reported a decrease in the gas layer thickness with increasing Re. By measuring the drag reductions and comparing the results to theoretical predictions, Rajappan et al. 46 reported the critical wall friction for the onset of gas depletion for several randomly roughed SHSs.

In this paper, we aim to gain a further understanding of the impact of surface roughness on the drag reduction as well as the plastron stability of SHS in turbulent flows. A series of SHSs with roughness heights in the range of $4 < k_{rms} < 14 \, \mu \text{m}$ (or $0.2 < k_{rms}^+ < 4.1$) were fabricated by spraying coating hydrophobic nano-particles on sandpaper. Different values of k_{rms} were obtained by varying the grit size of the sandpaper. The fabricated SHSs were tested in a fully developed turbulent channel flow facility, where the Reynolds number varies from $\sim 10\,000$ to $\sim 24\,000$. The skin friction drag of SHS was measured by pressure drop in the fully developed region. The status of the gas layer on SHS was monitored by a reflected light microscopy technique. The work was innovative compared to previous studies for the following reasons. First, a new method based on sandpaper was used to fabricate SHS. This method allowed us to systemically vary the roughness height of SHS and allowed us to create a sufficiently large

TABLE I. Summary of previous experimental studies on the impact of surface roughness on the drag reducing property of SHSs in turbulent flows (k_a : arithmetical mean roughness $k_a = \frac{1}{l} \int_0^l |h - \bar{h}| dx$, k_{ms} : root mean square roughness $k_{rms} = \sqrt{\frac{1}{l} \int_0^l |h - \bar{h}|^2 dx}$, and h is the roughness height.).

References	SHS fabrication methods	Surface roughness (μm)	k_{rms} or k_a in wall units	Measurement techniques	Drag reduction
Bidkar et al. ²²	Thermal spray	k _a : 1.1–15.6	0.06- 5.8	Force load	-50% to 30%
Ling et al. ⁴	Spray coating	k_{rms} : 4.8–20.4	0.43-3.28	Near-wall velocity	-10% to 36%
Gose et al. ²¹	Spray coating	k_{rms} : 1.2–18	0.15-4.5	Pressure drop	-90% to 90%
Rajappan et al. ⁴⁸	Acid-etching, spray coating	k_{rms} : 3.36–11	0.41-1.59	Torque	-2% to 26%
Abu Rowin and Ghaemi ⁴⁷	Spray coating	k_{rms} : 4.9	0.26-0.35	Near-wall velocity	38%-42%
Reholon and Ghaemi ⁴⁵	Spray coating	k_{rms} : 10.2	0.4-1.38	Near-wall velocity	-5% to 25%
Current work	Sandpaper	<i>k</i> _{rms} : 4–14	0.2-4.1	Pressure drop	-35% to 47%

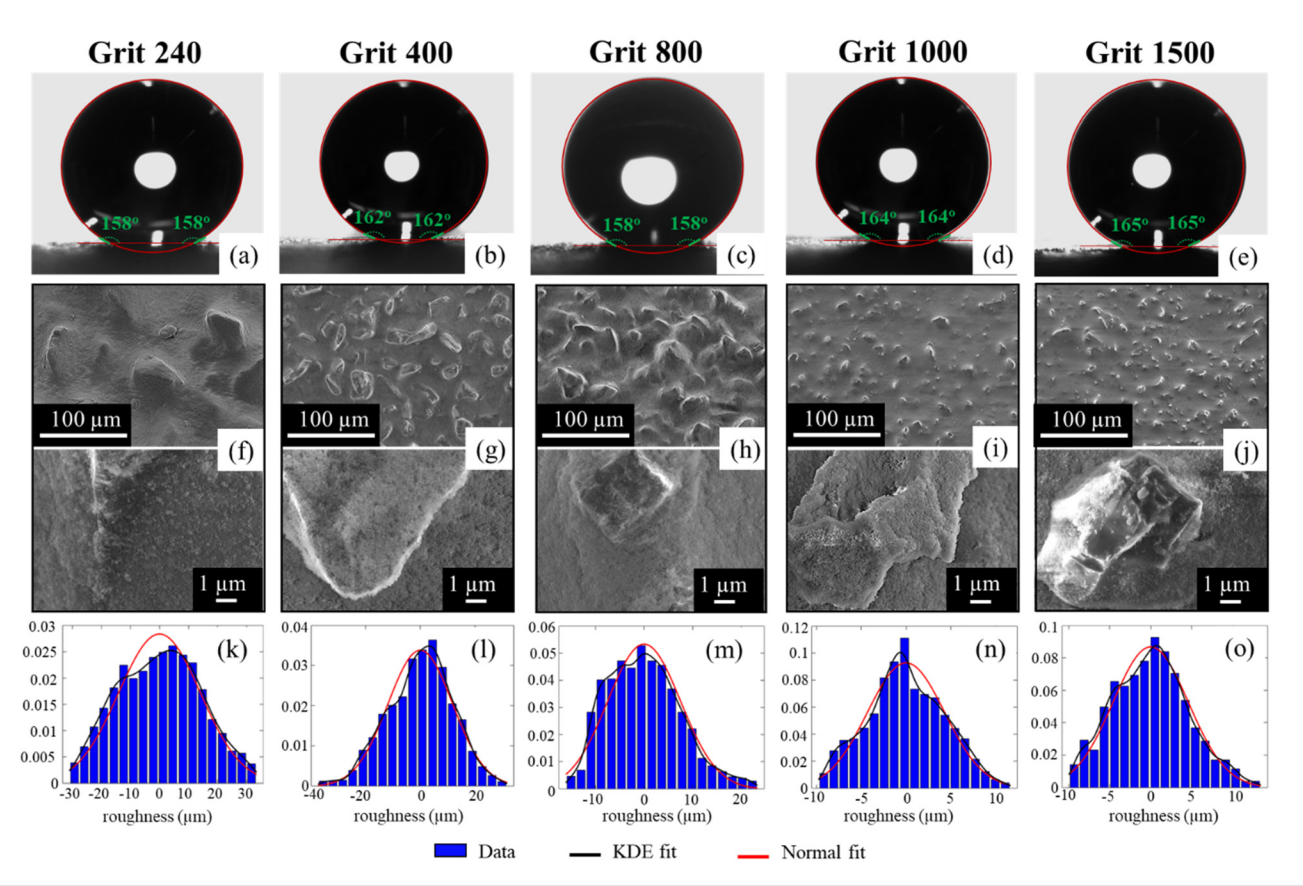


FIG. 1. Characterization of the five SHSs fabricated in this work including: (a)–(e) water contact angle, (f)–(j) SEM images of surface roughness, and (k)–(o) roughness height distributions.

SHS where the turbulent flows over SHS were fully developed. Second, a new method based on reflected light microscopy was implemented to monitor the plastron status in turbulent flows. This new method allowed us to quantitatively measure the variation of gas fraction at different Reynolds numbers. Third, it was the first time that the impact of roughness height on the plastron status in turbulent flows was investigated.

II. EXPERIMENTAL METHODS

A. Preparation of SHS with different roughness heights

SHSs are typically created due to a combination of surface roughness and hydrophobic chemistry. Following a method used in our previous work, ⁵⁴ we created SHSs with different roughness heights by spraying 30–50 nm silanized silica particles (Glaco Mirror Coat Zero from SOFT99 Corp) on sandpapers. Sandpapers with five different grit sizes: 240, 400, 800, 1000, and 1500 were used in this study. Prior to applying the nano-particles, the sandpapers underwent a cleaning process using an ultrasonic bath. Subsequently, they were dried and securely affixed to a flat plate to guarantee their flatness. Next, the nano-particles were dispersed evenly across the entire surface of the sandpaper through spraying. Finally, the sample was left to dry for one day in preparation for subsequent experiments. Figures 1(a)–1(e) show a water droplet seating on the coated surfaces with a contact

angle larger than 150° . The values of the water contact angle are listed in Table II.

The Scanning Electron Microscopy (SEM) images shown in Figs. 1(f)–1(j) demonstrate that the fabricated SHSs consisted of both microscale surface roughness corresponding to the abrasive particles on sandpapers and nanoscale surface roughness resulting from the silica nano-particle coatings. The wavelength and size of the abrasive particles, denoted as λ and d_p were estimated from the SEM images and listed in Table II. By increasing the grit size from 240 to 1500, d_p decreases from 42 \pm 12 to 7 \pm 3 μ m which agrees with previous studies, ^{54,55} as well as the ISO standards (ISO 6344-3)⁵⁶ and the sandpaper

TABLE II. Parameters of SHS including measured water contact angles (WCA), abrasive particles size (d_p) , k_{rms} , wavelength of abrasive particles (λ) , and gas fraction predicted by Cassie–Baxter model (φ_q) .

Grit size	240	400	800	1000	1500
WCA	158 ± 2°	162 ± 2°	158 ± 2 °	164 ± 2 °	165 ± 2 °
$d_p (\mu \mathrm{m})$	42 ± 12	18 ± 10	17 ± 6	10 ± 6	7 ± 3
k_{rms} (μ m)	14.2	8	7.2	4.7	4.6
λ (μm)	67 ± 14	28 ± 3	33 ± 9	24 ± 8	12 ± 2
Predicted φ_g	0.86	0.9	0.86	0.92	0.94

grit chart by Grainger.⁵⁷ For example, according to the sandpaper grit chart,⁵⁷ the sandpaper with a grit size of 240 has a nominal particle diameter of $40.5-58.5 \mu m$, which is very close to the value of $42\pm12\,\mu m$ found in our study. We further used a surface profiler (Bruker DektakXT^{TM} stylus, resolution in surface normal direction $0.1 \,\mu\mathrm{m})$ to measure the surface roughness. The measurement was repeated over five different locations, each covering a length of 2-5 mm. The probability density distributions (PDF) of roughness height (deviated from the average height, denoted as h) as well as the kernel density estimate (KDE) and the normal distribution fitting are plotted in Figs. 1(k)-1(o). The slight discrepancy between KDE and the normal fitting for all grit sizes indicates that the surface roughness of all current SHSs had non-Gaussian behavior, in agreement with those reported in Refs. 55 and 58. Figures 2(a) and 2(b) compare the PDFs of h for the five SHSs of different grit sizes, showing that a larger grit size leads to a smaller roughness height. The value of k_{rms} , as listed in Table II and shown in Fig. 2(c), reduced from 14.2 to 4.6 μm as increasing grit size from 240 to 1500, which was consistent with those reported in previous studies. 55,59,60 In the following, we use k_{rms} to characterize the surface roughness of sandpaper for the reasons that (i) the PDFs for h/k_{rms} for the five SHSs almost overlap with each other [Fig. 2(b)]; and (ii) the values of k_{rms}/d_p and k_{rms}/λ do not vary significantly [Figs. 2(d) and 2(e)].

Since the fraction of surface area covered by gas (i.e., gas fraction) φ_g is an important parameter determining the amount of drag reduction, we estimated the gas fraction for the fabricated SHS based on the Cassie–Baxter model: $\cos\theta = (1-\varphi_g)\cos\theta_0 - \varphi_g$, where θ is the measured water contact angle on SHS (these listed in Table II) and θ_0 is the contact angle on a flat surface with same surface chemistry of the SHS. Given the most hydrophobic material has a contact angle on the flat surface of about 120°, we used $\theta_0 = 120^\circ$. We estimated the gas fraction on the fabricated SHSs varies from 0.85 to 0.95, as listed in Table II. It should be noted that φ_g listed in Table II only applies to static conditions. As will be shown later, when the SHSs were subjected to turbulent flows, φ_g will be reduced.

B. Turbulent channel flow facility

The drag-reducing performance of the fabricated SHSs was measured in a fully developed turbulent channel flow facility, as shown in Fig. 3. The flow was driven by a 3-horsepower centrifugal pump. The flow rate was measured by an electromagnetic flowmeter (Omega Engineering, Inc., USA, range 2.2-150 gal/min, accuracy ±0.5% full range). Upstream of the channel, a settling chamber containing honeycombs and screens followed by a 10:1 contraction was used for controlling and reducing the inflow turbulence level. On the downstream side, a mild diffuser with an expansion angle of less than 7° links the channel with the main loop. At the inlet of the channel, spanwise tripping grooves were machined on the walls to force early boundary layer transition to turbulence. The channel's internal dimensions are 1016 \times 50 \times 6.4 mm³ (length \times width \times height). We denote the channel height as H, i.e., H = 6.4 mm. The turbulent flow in the channel is expected to be two-dimensional due to the 8:1 aspect ratio. 61,62 It should be noted that the channel height (H) was ensured to vary by less than 5% over the length of the channel and among different tested samples. For each test (SHS or smooth surface), before running the water tunnel, we measured channel height at five different streamwise locations by taking high-resolution images with a known spatial calibration.

A 50 mm wide and 880 mm long SHS (covering 86% of the length of the test section) was installed at the top wall of the test section. The 880 mm long SHS was obtained by joining four short pieces of SHS, as shown in Fig. 3(b). To ensure a fair comparison, our baseline was also created by joining four short pieces of smooth surface in a similar way. As shown in supplementary material Fig. S1, the joints for the smooth surface had a mismatch of 190 \pm 110 μ m in wall-normal directions, and the joints for SHS had a mismatch of $175 \pm 175 \,\mu$ m in both streamwise and spanwise directions. This mismatch was caused by the uncertainties in the fabrication and installation of samples. As will be shown later, the joints caused larger pressure drops in the channel compared to a wall with no joints. The mean flow speed in the test section, U_{mv} varies from 0.5 to 4.4 m/s. The Reynolds number (Re_m) based on the channel height and mean flow speed varies from 3400 to 26 400.

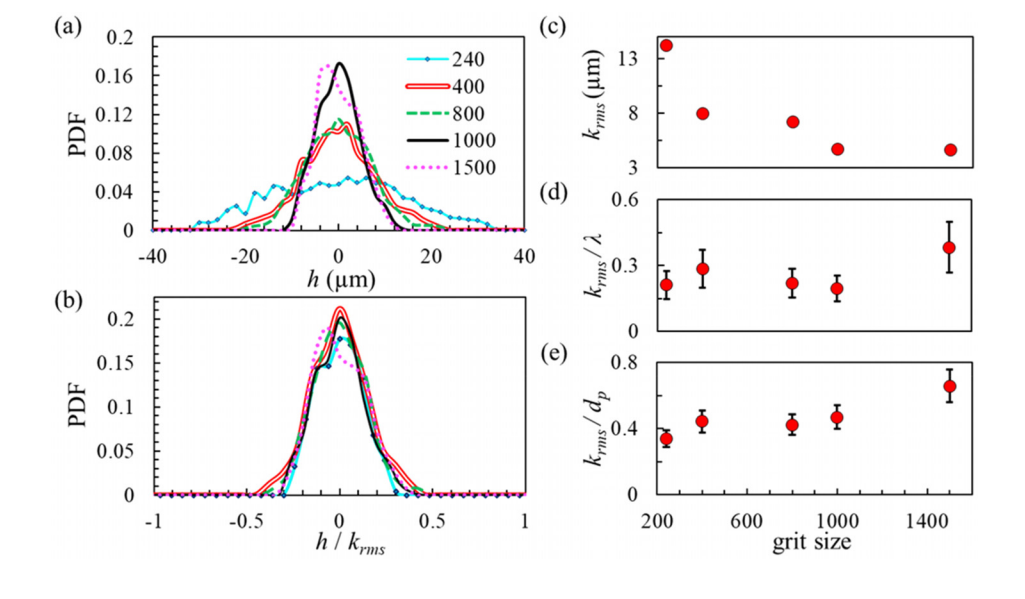


FIG. 2. PDF profiles of (a) h and (b) h/k_{rms} for the firve SHSs, and values of (c) k_{rms} , (d) k_{rms}/λ , and (e) k_{rms}/d_p as a function of grit size of SHSs.

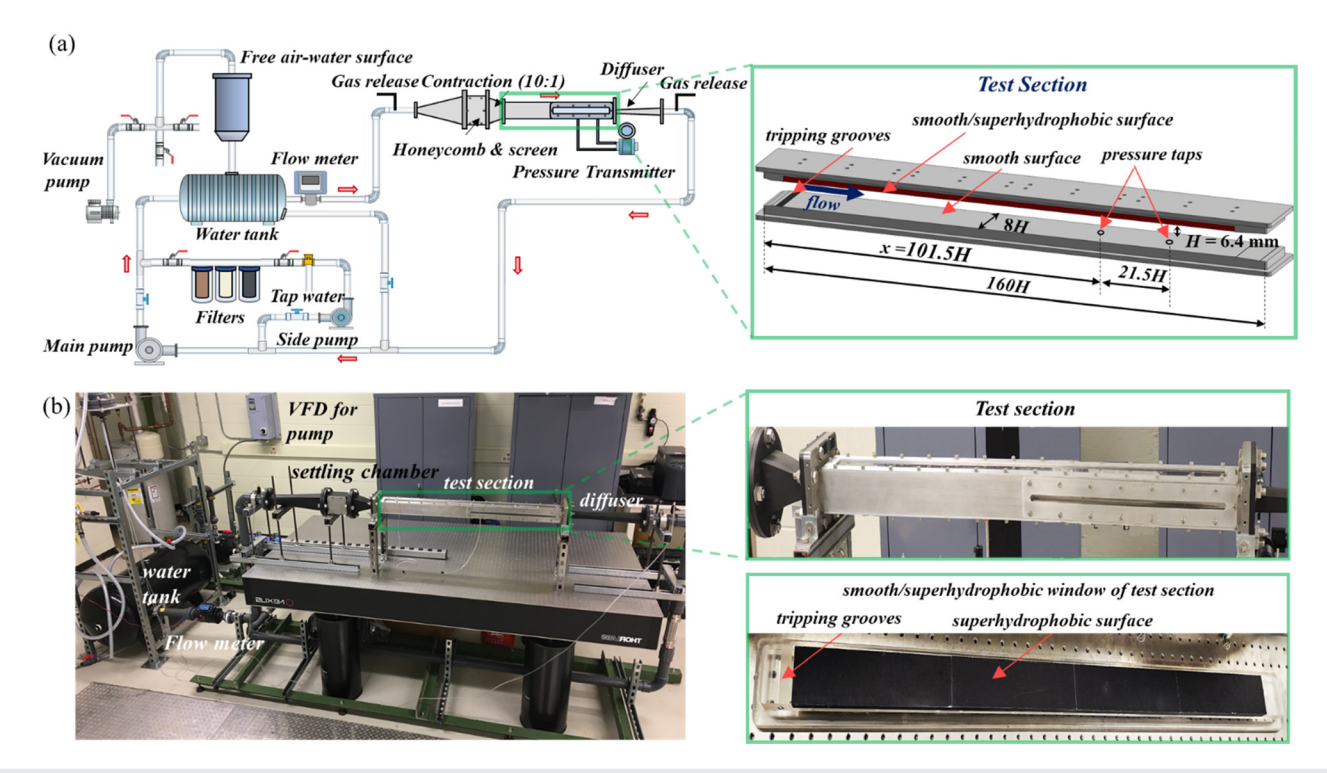


FIG. 3. (a) Schematic of the fully developed turbulent flow facility, and (b) images of the flow facility and the test section window where the SHS was installed.

The working fluid was water and was stored in a 60 gal storage tank. Prior to the experiments, the water passed through a three-level water purification system including 20, 5, and 1 μ m filters. We ran the water purification system for at least 24 h to ensure most particles were removed. In addition, the water was ensured to be saturated with air at atmospheric pressure, which was achieved by mixing the water with air at atmospheric pressure and keeping the water in the tank for at least two days. The saturation level of air in the water, measured by an optical oxygen sensor (FirestingO₂, Pyro Science), was $s = c/c_{atm} = 99\% \pm 3\%$, where c and c_{atm} denote the air concentrations measured by the sensor and for water saturated with air at atmosphere pressure, respectively. It should be noted that the experiments were carried out after any trapped air in the water tunnel was removed.

To isolate the impact of pressure on the testing result, we maintain the hydrostatic pressure at the inlet of the test section as $(1.10\pm0.01)\times10^5$ Pa by carefully adjusting the height of the free airwater interface above the test section.

C. Measurement of drag reduction and plastron status

Following Ref. 21, the drag reduction of the SHSs was measured based on the pressure drops in the test section at the fully developed region. The pressure drop Δp was measured from two tap holes (diameter 0.75 mm, depth of 3.0 mm) located at streamwise distances of 101.5H and 123H (distance between two holes was L=21.5H) from the channel inlet, respectively, and via a differential pressure transmitter (Omega Engineering, #PX3005-160WDWBI, range 80 kPa, precision 0.075%). Once the pressure drop was determined, the skin friction τ_{wz} skin friction coefficient

 $C_{f^{\sharp}}$ and drag reduction DR were calculated by the following three equations, respectively, as

$$\tau_w = -\frac{H}{2} \frac{\Delta p}{L},\tag{1}$$

$$C_f = \frac{\tau_w}{0.5\rho U_m^2},\tag{2}$$

$$DR = 2 \times \left(1 - \frac{C_f}{C_{f0}}\right),\tag{3}$$

where ρ is the density of water, and C_{f0} denotes the skin-friction coefficient measured on a smooth surface at the same Reynolds number. In the following, a subscript 0 will be used to denote quantities measured on a smooth wall. The factor of two in Eq. (3) arises as only one of the two channel walls is SHS.⁶³

To visualize the plastron while the SHS was subjected to turbulent flows, we used the reflected light microscopy technique as shown in Fig. 4. A collimated LED light (Thorlabs, model #M625L4-C4, wavelength 632 nm) was used as the illumination source. The light was directed through a beam splitter to an objective (Edmund, model #46-144, $10\times$, infinity corrected, working distance 34 mm) in the direction perpendicular to the sample. A CMOS camera (FLIR, model #GS3-U3-41C6M-C, 2048×2048 pixels) was used to record the light reflected from the SHS. Figures 4(b) and 4(c) show two images recorded using this setup at static conditions. Figure 4(b) corresponds to a purely rough surface (uncoated sandpaper), and Fig. 4(c) is for an SHS (sandpaper coated by hydrophobic nanoparticles). The air layer attached to the SHS can be clearly observed.

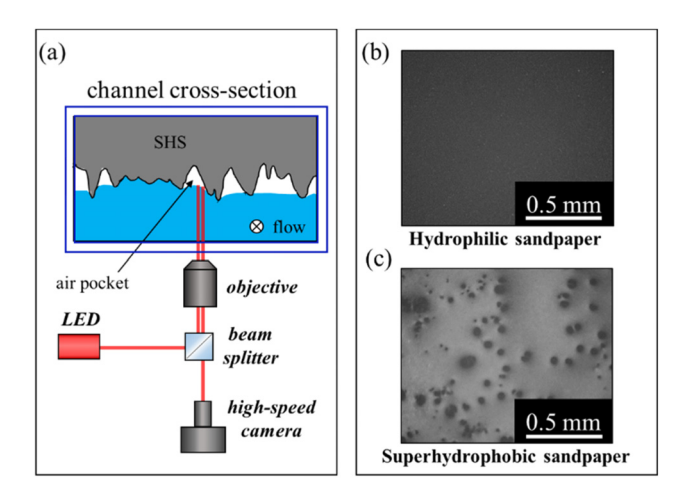


FIG. 4. (a) Optical setup for visualizing plastron statue on SHS, two sample images obtained by the setup corresponding to (b) an uncoated sandpaper and (c) an SHS with a grit of 800.

III. RESULTS

A. Comparison of wall frictions on a smooth wall, SHS, and uncoated sandpaper

First, we show the measurement results for an SHS with a grit size of 1000, where k_{rms}^+ was in the range of 0.52–1 and the surface roughness effect was negligible. We compared the results to a smooth

surface as well as to an uncoated sandpaper with the same grit size of 1000. Figures 5(a) and 5(b) show the pressure drop and C_f for the three surfaces, respectively. Figure 5(c) shows DR as a function of Re_m . The empirical relation $C_f = 0.0743 Re_m^{-0.25}$ for turbulent channel flows over a smooth wall provided by Zanoun $et\ al.^{62}$ was also plotted in Fig. 5(b) for comparison. Our result showed that the C_f of the smooth wall was about 60% higher than the prediction by the empirical relation. The reason for the higher C_f on the smooth wall was due to the five joints between short samples (supplementary material Fig. S1). As mentioned earlier, the joints had a mismatch of 190 \pm 110 μ m in wall-normal direction and acted like tripping grooves. As shown in supplementary material Fig. S2, we found that a smooth wall with no joints had C_6 which agreed very well with the empirical relation.

The uncoated sandpaper had slightly higher pressure drops and C_f compared to those measured on the smooth wall. The amount of drag increase by the sandpaper compared to the smooth wall was about 10%. The reason for a mild 10% drag increase by this sandpaper is likely due to the small value of k_{rms}^{+} which was in the range of 0.5–1. The maximum peak-to-trough roughness height for this sample is $h_{PT}=22.6~\mu \mathrm{m}$ (or $h_{PT}^{+}<5$), which falls in the transitional rough region. Similar results were observed in the literature. Signology For example, Flack and Schultz of found no drag increase for rough surfaces with k_{rms}^{+} close to 1.

The SHS had the lowest C_f compared to the smooth wall and uncoated sandpaper. Figure 5(c) shows the drag reduction as a function of Re_m . The SHS provided nearly a constant 47% drag reduction compared to the smooth wall at the current range of Re_m [Fig. 5(c)]. Considering that the only difference between SHS and uncoated

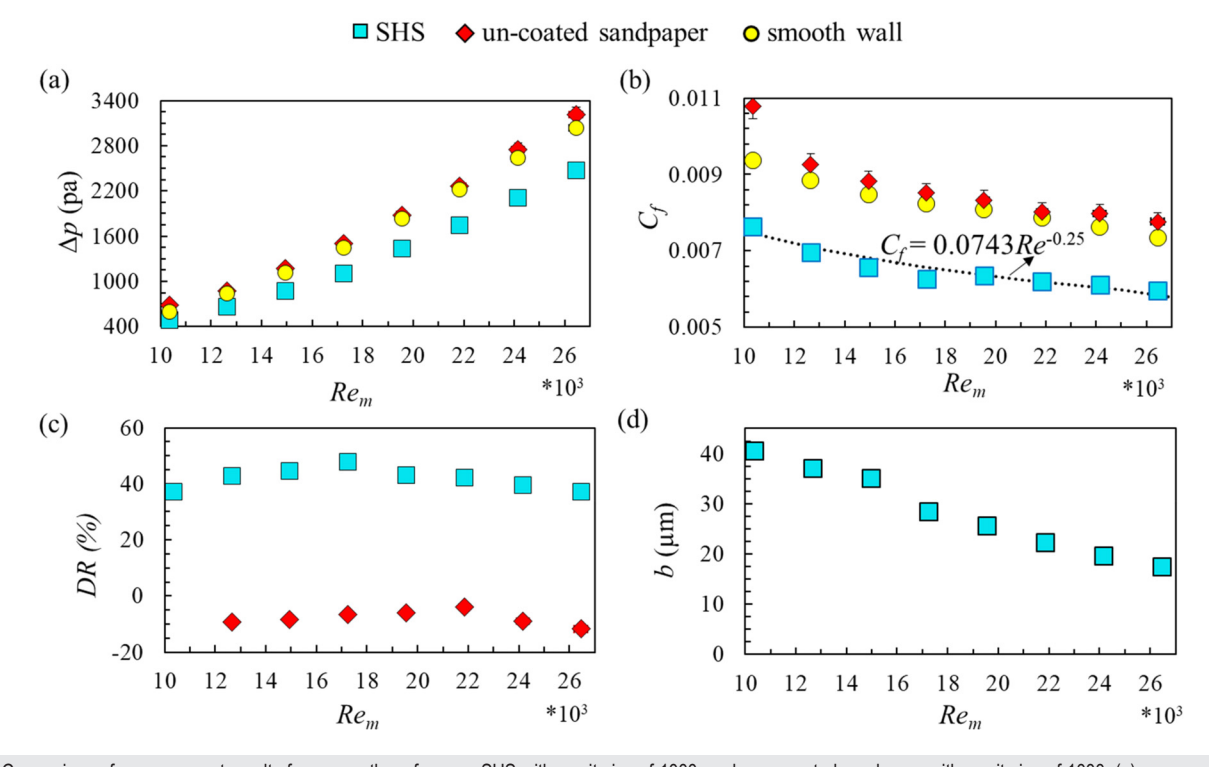


FIG. 5. Comparison of measurement results for a smooth surface, an SHS with a grit size of 1000, and an uncoated sandpaper with a grit size of 1000: (a) pressure drop, (b) C_f , (c) DR, and (d) slip length. The error bar is smaller than the size of the symbols.

sandpaper is the presence of gas on the SHS, our result confirmed that the drag reduction by SHS was due to the trapped gas.

The drag reduction of SHS in turbulent flows was mainly due to the slip velocity, 14 and finite slip velocities on SHS were experimentally measured by many authors. 66,67 Thus, to understand why DR was nearly constant and independent of the Reynolds number, we assumed the SHS was an effective slip boundary and estimated the slip length b based on the measured drag reduction. According to the model proposed by Fukagata $et\ al.$, 68 a relationship between DR and b can be obtained by matching the bulk mean velocity of the no-slip flow to that of the slip flow as

$$u_{\tau 0} \left(\frac{1}{k} \log(Re_{\tau}u_{\tau 0}/u_{\tau}) + F\left(b_{y}^{+} = 0\right) \right)$$

$$= u_{\tau} \left(b_{x}^{+} + \frac{1}{k} \log(Re_{\tau}) + F\left(b_{y}^{+}\right) \right), \tag{4}$$

where k=0.41 is the von Kármán constant, $u_{\tau}=(\tau_w/\rho)^{0.5}$ is the friction velocity, $Re_{\tau}=u_{\tau}\delta/\nu$ is the friction Reynolds number, b_x and b_y denote the slip length in the streamwise and spanwise direction, and $F(b_y^+)$ is an empirical function depending on b_y^+ (here, we used the empirical relation proposed by Busse and Sandham²⁴). Furthermore, we assumed $b_x=b_y$ considering the current SHS had a random texture. The estimated slip length is shown in Fig. 6(d). Clearly, the slip length reduced as increasing Re_m . A similar trend has been

observed in the experimental work by Rowin and Ghaemi⁴⁷ who measured the slip length based on the velocity profile close to SHS, and in the numerical simulations by Seo and Mani.⁶⁹ The reduction of slip length with increasing Re_m could be possibly attributed to larger interface vibration.⁴⁷ It should be noted that the gas fraction was nearly constant at $10\,000 < Re_m < 24\,000$ as will be shown later. Thus, the reduction of b is not due to the reduction of the gas fraction.

B. Impact of surface roughness on drag reducing performance of SHS

Figures 6(a)–6(c) show the experimentally measured C_f , DR, and k_{rms}^+ as a function of Re_m , respectively, for the five SHSs with grit sizes varying from 240 to 1500. Clearly, for SHSs with grit sizes of 800 and 1500 (or small roughness height $k_{rms}^+ < 1$), the trends are very similar to those observed on the SHS with grit size of 1000: the drag reduction is nearly a constant as increasing Reynolds number. This is probably because the surface roughness effect is negligible on these surfaces.

For SHS with grit size of 400 which had a slightly larger roughness height (0.9 $< k_{rms}^+ < 1.9$) compared to SHSs with grit size larger than 800, the amount of drag reduction reduced from 41% to 17% as increasing Reynolds number from 10 000 to 24 000. This result indicates that the surface roughness of the sample with a grit size of 400 was large enough to influent the flow, and caused a lower drag

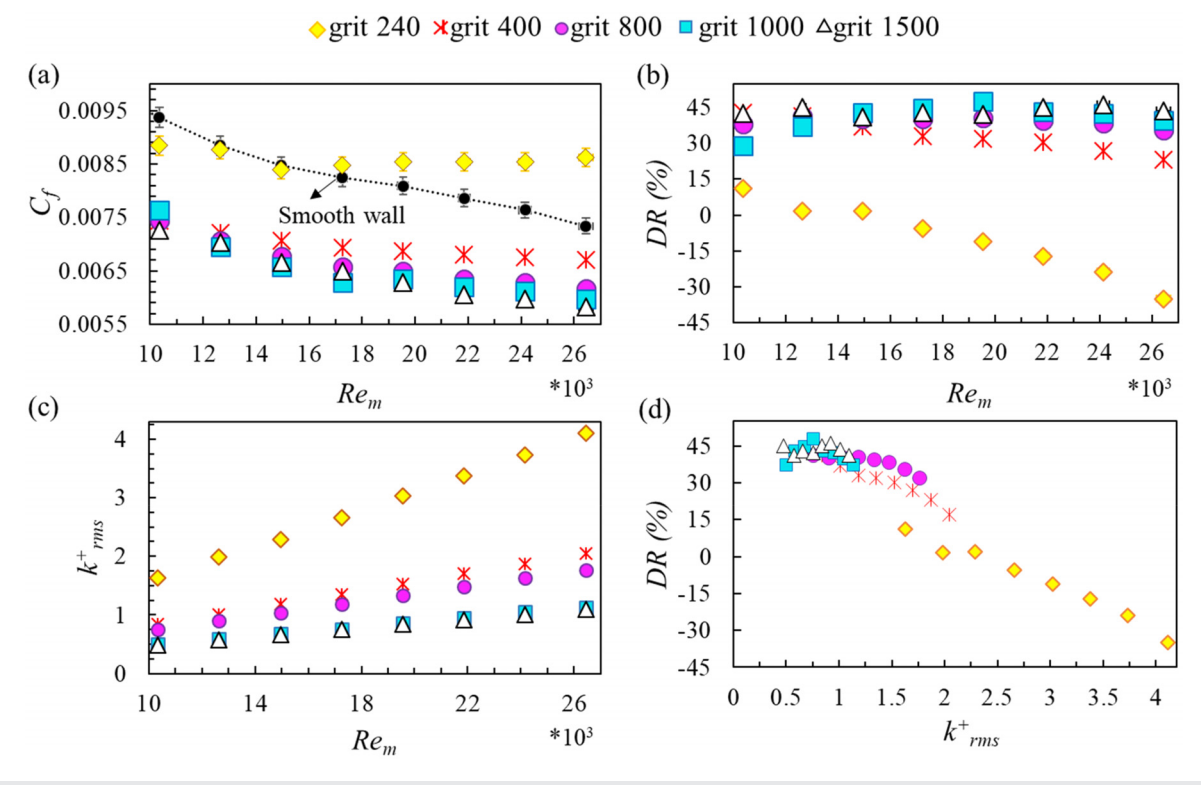


FIG. 6. Measurement results for the five SHSs with grit sizes ranging from 240 to 1500, including: (a) C_{f_1} (b) DR, (c) k_{rms}^+ , and (d) DR as a function k_{rms}^+ . The error bar is smaller than the size of the symbols.

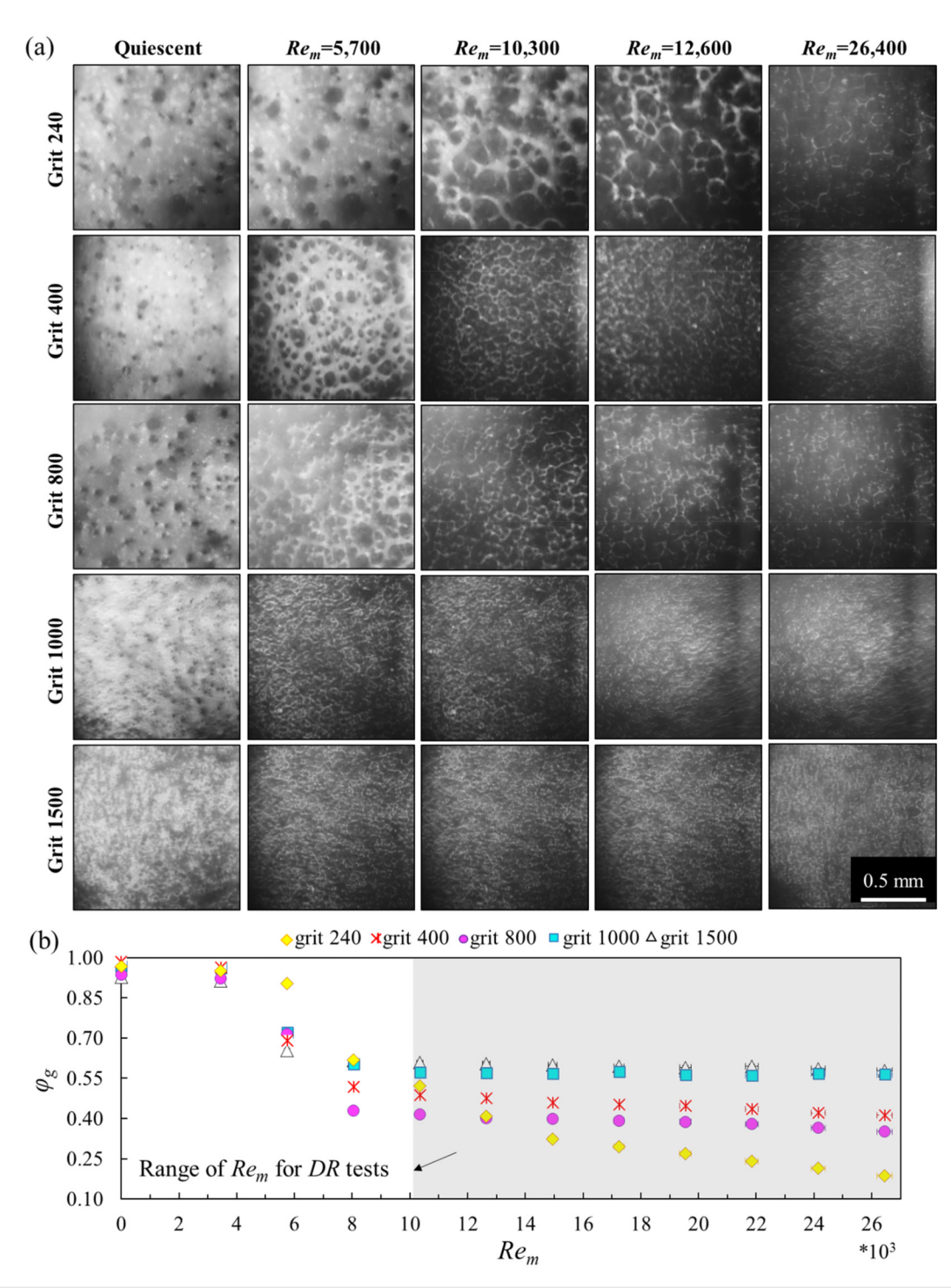


FIG. 7. (a) Raw images captured by the reflected light microscopy showing the status of the air layer on the five SHSs at different Re_m and (b) φ_q as a function of Re_m .

reduction by SHS as increasing Reynolds number. Noted that the depletion of the gas layer at higher Reynolds numbers could also lead to a lower drag reduction by SHS. However, as shown later, for the SHSs in our work, φ_g was nearly a constant at the given range of

Reynolds numbers. Thus, we provide new evidence that surface roughness causes a lower drag reduction by SHS. ^{22,45}

For SHS with the smallest grit size of 240, which has the largest roughness height (1.9 $< k_{rms}^+ <$ 4.1), no drag reduction was observed.

At low Reynolds numbers, the wall friction is similar to that of a smooth wall. As increasing Reynolds number, a higher percentage of drag increasing was observed. This behavior was similar to turbulent flows over a rough surface, where a higher drag increase as increasing Reynolds number is expected since the roughness height normalized by viscous wall unit becomes larger at larger Re_m . An increase in drag by SHS compared to a smooth wall due to large roughness height was also observed in other experimental works. 4,22

Finally, we found a strong correlation between DR and k_{rms}^+ as shown in Fig. 6(d), which confirmed the importance of surface roughness on the drag reducing performance of SHS. For SHSs with k_{rms}^+ < 1, as increasing k_{rms}^+ , the DR remains nearly constant. For SHSs with $1 < k_{rms}^+ < 2$, the amount of DR reduces as increasing k_{rms}^+ , and when $k_{rms}^+ > 2$, the SHS has no DR and has a higher percentage of drag increase as increasing k_{rms}^+ . The relationship between DR and k_{rms}^+ was very similar to those reported in Ref. 45.

C. Impacts of Reynolds number and surface roughness on plastron status

Figure 7(a) shows the raw images captured by the reflected light microscopy for the five SHSs at different Reynolds numbers. Figure 7(b) shows φ_g as a function of the Reynolds number. The value of φ_g was estimated based on the area of the bright region shown in these images. At stationary liquid ($Re_m=0$), the gas fraction on all SHSs, regardless of the roughness height, is about 0.96 \pm 0.03. Only a few largest roughness elements were exposed to water, and the gas–liquid interface formed between these largest roughness elements, in agreement with the observation by Reholon and Ghaemi. The high value of φ_g agreed with the theoretical estimations provided in Table I. Other studies have also shown high φ_g for SHS with random textures immersed in quiescent water.

When exposed to flow and increasing Reynolds number, φ_g reduced due to the shear and turbulence as expected. It should be highlighted that this is the first time that direct experimental evidence showing the reduction of gas fraction due to the effect of flow is provided. This result was consistent with the experimental data obtained

by Reholon and Ghaemi, ⁴⁵ who showed that the thickness of the plastron reduces as increasing Reynolds number.

However, the trends of how ϕ_g changed as increasing Re_m for SHSs with different grit sizes were very different. For SHSs with grit sizes smaller than 800, as Re_m increased, ϕ_g decreased gradually. For example, for SHS with grit size 240, φ_g slowly reduced from 0.96 to 0.14 as increasing Re_m from 0 to 26 000. For SHSs with grit sizes larger than 1000, as Re_m increased, φ_σ decreased more rapidly until it reached a stable value. For example, for SHS with grit sizes 1000 and 1500, $\phi_{\rm g}$ quickly dropped from 0.96 to 0.57 as increasing Rem from 0 to 7000 and was nearly a constant of 0.57 as Re_m continuously increased. Similar trends were also observed for the length scale of the gas pocket. Supplementary material Fig. S3 shows the maximum size of the gas pocket (g_{max}) and the corresponding capillary pressure $p^{Ca} = \gamma/g_{max}$ as a function of Reynolds number for two SHSs with grit sizes of 240 and 1000. As shown in supplementary material Fig. S3, for SHS with small grit size, g_{max} and p^{Ca} changed gradually. While for SHS with large grit size, g_{max} , and p^{Ca} quickly reached to a stable value. Moreover, the SHS with grit size 240 had smaller p^{Ca} compared to the SHS with grit size 1000, which might be the reason that caused the gas pocket to be less stable and the gas fraction to reduce continuously.

The possible reason for these different trends could be explained by the schematic drawings shown in Fig. 8. The cross section represents the surface texture obtained by the surface profiler, and the water meniscus formed between different roughness peaks. As shown in supplementary material Fig. S4(a), the SHS with a small grit size (or large k_{rms}^{+}) has roughness elements with a peak height h_p (measured from the lowest point) ranging from 10 to 50 µm. Consequently, the airwater interface could pin to the roughness elements with intermediate roughness heights before reaching the smallest textures, and the gas fraction reduces gradually. In contrast, as shown in supplementary material Fig. S4(b), the SHS with a large grit size (or small k_{rms}^{+}) has a small range of h_p from 5 to 30 μ m. Thus, there were fewer intermediate roughness elements facilitating the pinning of air-water interface similar to the SHS with smaller grit sizes. A similar multi-stage reduction of gas fraction due to turbulent flows over SHS has also been observed by Sakai et al.7

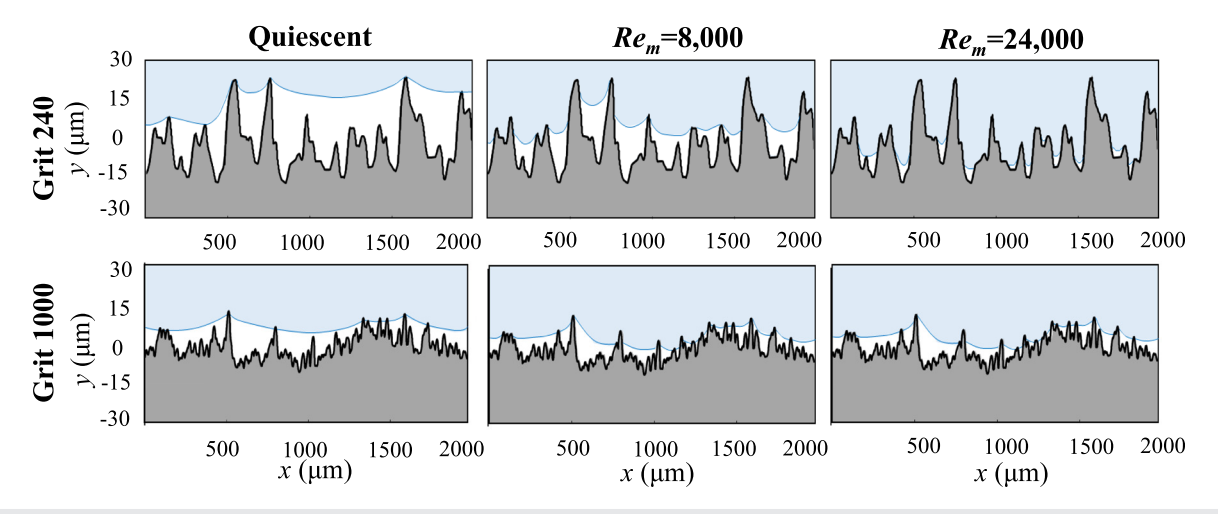


FIG. 8. Schematic representation of the air layer status on SHS as increasing Re_m (height distributions of SHS were obtained by a surface profiler).

Comparing SHSs with different grit sizes, we found that at small Reynolds numbers ($Re_{\rm m} < 7000$), the SHSs with smaller grit sizes had a larger φ_g in comparison with those with larger grit sizes. As explained earlier, the reason was possibly because of the presence of intermediate roughness elements which facilitated the pinning of the air–water interface. However, at higher Reynolds numbers ($Re_{\rm m} > 15\,000$), the SHSs with larger grit sizes promoted a larger φ_g . The possible reason was that the SHS with a larger grit size had a smaller texture spacing, and a larger interface curvature when the interface deforms, and thus allowed the plastrons to sustain a higher pressure fluctuation in turbulent flows. The trend that an SHS with a smaller texture spacing promotes a more stable plastron in turbulent flows has also been reported in a few numerical simulations.

Finally, to explain why the current SHSs could sustain the plastron at the highest Re_m (e.g., why the SHS with a grit size of 1000 maintained a nearly constant $\varphi_g = 0.57$ as increasing Re_m), we estimated the maximum pressure difference (p^{max}) that can be sustained by the gas-liquid interface and compared it to the maximum wall shear stress (τ_w) applied on the SHS at $Re_m = 24\,500$ [obtained based on pressure drop and Eq. (1)]. According to the model proposed by Seo *et al.*, ^{26,52} gas depletion occurs when $p_{w,rms} > p^{max}$, where $p_{w,rms}$ is the rms value of wall pressure fluctuation on the SHS. Assuming $p_{w,rms}$ falls in the range of $5-10\tau_w$ for turbulent flows over SHS, ⁵² gas depletion is expected when τ_w/p^{max} is larger than a critical value of 0.1 or 0.2.

We estimated the value of p^{max} based on the force-balance equation at the gas-liquid interface as⁷⁴

$$p^{max} = \gamma L_p |\cos \theta_{adv}| / \varphi_{\varrho} \lambda^2, \tag{5}$$

where φ_g λ , and L_p are the three geometrical parameters of SHS texture: gas fraction, texture wavelength, and texture perimeter, respectively, θ_{adv} is the local advancing contact angle (i.e., the contact angle when interface de-pins from the tip of the roughness elements), and $\gamma = 72 \times 10^{-3}$ N/m is the surface tension of water. As shown by Ling et al., the value of θ_{adv} for SHS with a combination of microscale/nanoscale roughness was as large as 150°. Thus, we assumed $\theta_{adv} = 150^\circ$ for current surfaces. To estimate L_p , we approximated the SHSs with an array of circular posts of the same diameter of the abrasive particles, so that $L_p = \pi d_p$. The value of φ_g was directly obtained based on Fig. 7 corresponding to the highest Reynolds

number ($Re_m = 24\,500$). Figures 9(a) and 9(b) plot the value of p^{max} and τ_w/p^{max} , respectively, as a function of grit size. Clearly, the value of τ_w/p^{max} is much smaller than the critical value of 0.1 or 0.2. Therefore, the persistence of air pockets on current SHSs in turbulent flows is explained.

D. Comparison of experimentally measured drag reduction with models

In this section, we attempted to understand why the three SHSs (grit sizes of 800, 1000, and 1500) had similar drag reduction, and whether the amount of drag reduction can be predicted by past theoretical models. In general, the drag reduction of SHS depends on both λ^+ and φ_g , and a larger drag reduction could be obtained by either increasing λ^+ or increasing φ_g .

Figures 10(a) and 10(b) shows the drag reduction as a function of λ^+ and φ_g . The value of λ was obtained from SEM images and defined as the average spacing between roughness elements. The values of φ_g were obtained by reflective microscopy as shown in Fig. 7. The effects of λ^+ and φ_g on the drag reduction observed for the SHSs with three grit sizes were expected. The SHSs with a larger grit size (i.e., a smaller λ^+) generally had a larger gas fraction (0.35 $<\varphi_g<$ 0.41 for grit size 800, $\varphi_g\approx$ 0.57 for grit size 1000, and $\varphi_g\approx$ 0.60 for grit size 1500). Therefore, as increasing the grit size, the opposite effects of larger φ_g and smaller λ^+ lead to nearly constant drag reductions observed on the three SHSs.

Figures 10(c) and 10(d) compared the experimentally measured drag reduction to two theoretical models. In the first model shown in Fig. 10(c), the drag reduction was predicted based on the empirical models proposed by Rastegari and Akhavan²⁶ as

$$(1-DR) = \{1 + \left[1/(2\kappa) \ln(1-DR) + (B-B_0)\right] (C_{f0}/2)^{0.5} \}^{-2},$$
(6a)

$$(B-B_0) = 0.41\{(\varphi_g)(1-\varphi_g)^{-3/8}\}\{g^+\}^{3/4}, \tag{6b}$$

where $(B-B_0)$ is the upward shift of the mean velocity profile in the log region compared to the smooth wall, and $g^+=g/\delta_\nu$ is the width of texture indentations expressed in wall unit. Here, we estimated $g=\lambda-d$. In the second model shown in Fig. 10(d), we first estimated the slip length according to the model proposed by Seo and Mani⁶⁹ as

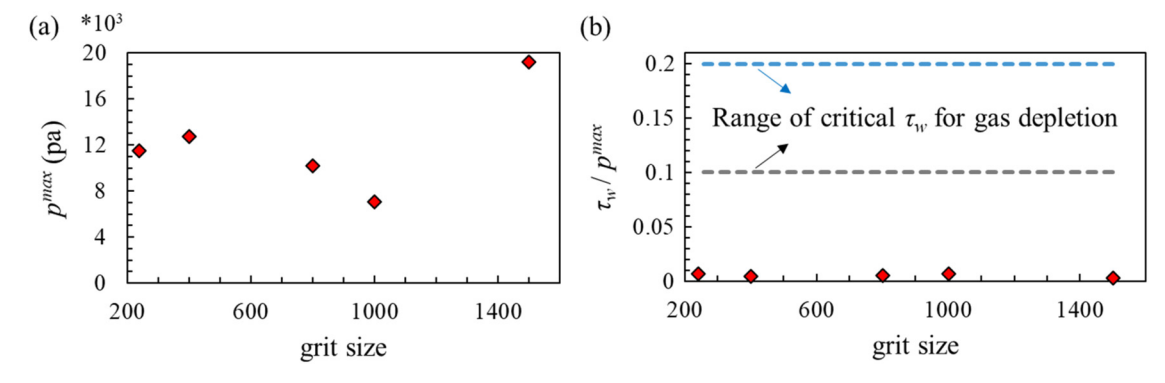


FIG. 9. (a) p^{max} for the five SHSs estimated by Eq. (5), and (b) comparison of the estimated τ_w/p^{max} for the five SHSs with the critical values for the onset of gas depletion by turbulence

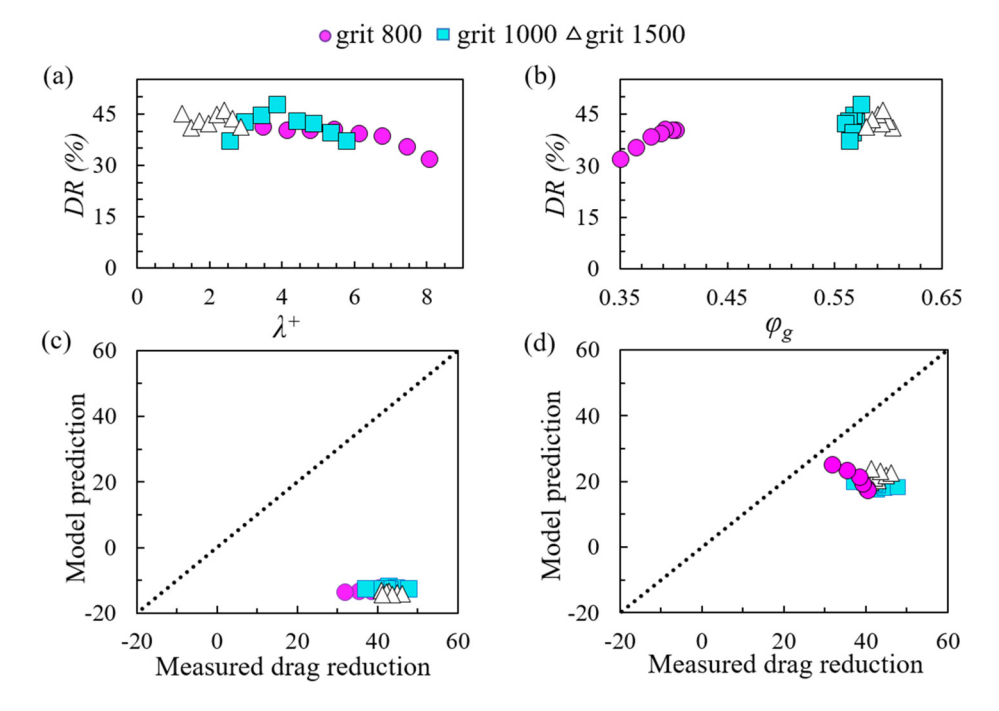


FIG. 10. (a) and (b) Drag reduction as a function of λ^+ and φ_{g_i} (c) and (d) comparison of the experimentally measured drag reduction to the predictions by models. (c) is based on a model by Rastegari and Akhavan²⁰ and (d) is based on a model by Seo and Mani. ⁵⁹

$$\lambda^{+} = b^{+}/C_{b} + 0.328 (b^{+})^{3} (1 - \varphi_{g})^{3/2},$$
 (7)

where $C_b=0.325/(1-\varphi_g)^{0.5}-0.44$. This model was obtained by fitting simulation results for turbulent flows over SHSs with $6<\lambda^+<310$ and $8/9<\varphi_g<63/64$. After obtaining b^+ , the drag reduction was estimated by assuming $b_x=b_y$ and using Eq. (4). As shown in Figs. 10(c) and 10(d), both models predicted a lower drag reduction compared to the experimental measurements. Again, the possible reason might be due to the complex texture geometry of the randomly roughed SHSs used in this work. Another possible reason for the disagreement between experiments and the model by Seo and Mani was that Eq. (7) was developed for SHSs with large gas fractions ($\phi_g>0.8$) and thus was not suitable for current SHSs with relatively small gas fractions ($0.35<\phi_g<0.6$). The morphology of the gas on the randomly roughed SHS may not be simply represented by λ and ϕ_g .

IV. CONCLUSION

In summary, by using SHSs with different sandpaper grit sizes, we studied the impact of surface roughness on drag reduction as well as the plastron stability of SHSs in turbulent channel flows. We measured the drag reduction based on the pressure drops. We found that the drag reducing property of SHS heavily depended on the roughness height. For SHSs with $k_{rms}^+ < 1$, the roughness effect was negligible, and the drag reduction remained nearly constant as increasing Reynolds number and k_{rms}^+ . A maximum 47% drag reduction was observed. For SHS with $1 < k_{rms}^+ < 2$, the roughness effect cannot be neglected, less drag reduction was observed as increasing Reynolds number and k_{rms}^+ . When $k_{rms}^+ > 2$, the roughness effect overcame the slip effect of the SHSs, resulting in a drag increase.

Furthermore, we measured the plastron status based on highresolution imaging. We found a reduction of gas fraction due to the effect of flows: the gas fraction was about 0.9 in stationary liquid but reduced to less than 0.6 underflows. We found that the surface roughness greatly influenced the trend of plastron depletion in turbulent flows. For SHS with large k_{rms} , as increasing Reynolds number, φ_g reduced gradually, probably due to the pinning of gas–liquid interface at roughness elements with intermediate roughness heights. For SHS with small k_{rms} , as increasing Reynolds number, φ_g reduced rapidly and maintained a constant value. We found that the SHS with smaller k_{rms} has a larger φ_g in high-Reynolds number turbulent flows, suggesting that smaller roughness features promote a more stable plastron due to the larger surface tension. Our results also showed that as increasing Re_m , the slip length of SHS reduced, although φ_g was a constant. The reduction of slip length might be due to the interface vibration at high Reynolds number flows.

We believe our results provided a better understanding of the surface roughness effect on the performance of SHSs in turbulent flows. Our results could guide the design, fabrication, and implementation of SHS for reducing drag in large-scale applications, such as marine ships. Future works are required to further understand the dynamics of the gas-liquid interface in turbulent flows, the mechanism of slip length reduction as increasing Reynolds number, and to develop a predictive model of drag reduction for SHS with randomly roughed textures.

SUPPLEMENTARY MATERIAL

See the supplementary material includes supplementary material Figs. S1-S4.

ACKNOWLEDGMENTS

We thank the support of National Science Foundation (Grant No. 2041479) and UMass Dartmouth's Marine and Undersea Technology (MUST) Research Program funded by the Office of Naval Research (ONR) (Grant No. N00014-20-1-2170). We also thank Paul Sousa for the assistance of fabricating the experimental

AUTHOR DECLARATIONS

Conflict of Interest

The authors have no conflicts to disclose.

Author Contributions

Shabnam Mohammadshahi: Data curation (equal); Formal analysis (equal); Investigation (equal); Methodology (equal); Writing - original draft (equal). Daniel O'Coin: Data curation (equal); Investigation (equal). Hangjian Ling: Conceptualization (equal); Funding acquisition (equal); Supervision (equal); Writing - original draft (equal); Writing - review & editing (equal).

DATA AVAILABILITY

The data that support the findings of this study are available from the corresponding author upon reasonable request.

REFERENCES

- ¹B. Bhushan and Y. C. Jung, "Natural and biomimetic artificial surfaces for superhydrophobicity, self-cleaning, low adhesion, and drag reduction," Prog. Mater. Sci. 56, 1–108 (2011).
- ²S. S. Ganar and A. Das, "Unraveling the interplay of leaf structure and wettability: A comparative study on superhydrophobic leaves of Cassia tora, Adiantum capillus-veneris, and Bauhinia variegata," Phys. Fluids 35, 114113 (2023).
- ³J. Ou, B. Perot, and J. P. Rothstein, "Laminar drag reduction in microchannels using ultrahydrophobic surfaces," Phys. Fluids 16, 4635-4643 (2004).
- ⁴H. Ling, S. Srinivasan, K. Golovin, G. H. McKinley, A. Tuteja, and J. Katz, "High-resolution velocity measurement in the inner part of turbulent boundary layers over super-hydrophobic surfaces," J. Fluid Mech. 801, 670-703 (2016).
- ⁵M. S. Naim and M. F. Baig, "Turbulent drag reduction in Taylor-Couette flows using different super-hydrophobic surface configurations," Phys. Fluids 31, 095108 (2019).
- ⁶C. Neinhuis and W. Barthlott, "Characterization and distribution of waterrepellent, self-cleaning plant surfaces," Ann. Bot. 79, 667–677 (1997).
- ⁷Y. Liu, M. Wu, Z. Zhang, K. Luo, J. Lu, L. Lin, K. Xu, H. Zhu, B. Wang, W. Lei, and Y. Fu, "Fabrication of wear-resistant and superhydrophobic aluminum alloy surface by laser-chemical hybrid methods," Phys. Fluids 35, 052108
- ⁸A. Marmur, "Super-hydrophobicity fundamentals: Implications to biofouling prevention," Biofouling 22, 107-115 (2006).
- ⁹¹G. B. Hwang, K. Page, A. Patir, S. P. Nair, E. Allan, and I. P. Parkin, "The antibiofouling properties of superhydrophobic surfaces are short-lived," ACS Nano 12, 6050-6058 (2018).
- 10 A. M. A. Mohamed, A. M. Abdullah, and N. A. Younan, "Corrosion behavior of superhydrophobic surfaces: A review," Arab. J. Chem. 8, 749-765 (2015).
- ¹¹Y. Cheng, J. Xu, and Y. Sui, "Numerical study on drag reduction and heat transfer enhancement in microchannels with superhydrophobic surfaces for electronic cooling," Appl. Therm. Eng. 88, 71-81 (2015).
- ¹²P. Zhang and F. Y. Lv, "A review of the recent advances in superhydrophobic surfaces and the emerging energy-related applications," Energy 82, 1068-1087 (2015).
- 13 M. Kharati-Koopaee and M. R. Akhtari, "Numerical study of fluid flow and heat transfer phenomenon within microchannels comprising different superhydrophobic structures," Int. J. Therm. Sci. 124, 536-546 (2018).
- ¹⁴H. Park, C. H. Choi, and C. J. Kim, "Superhydrophobic drag reduction in turbulent flows: A critical review," Exp. Fluids 62, 229 (2021).
- 15C. Lee, C. H. Choi, and C. J. Kim, "Structured surfaces for a giant liquid slip," Phys. Rev. Lett. 101, 064501 (2008).

- ¹⁶C. Lee, C. H. Choi, and C. J. Kim, "Superhydrophobic drag reduction in laminar flows: A critical review," Exp. Fluids 57, 176 (2016).
- ¹⁷D. Song, R. J. Daniello, and J. P. Rothstein, "Drag reduction using superhydrophobic sanded Teflon surfaces," Exp. Fluids 55, 1783 (2014).
- 18^tT. Min and J. Kim, "Effects of hydrophobic surface on skin-friction drag," Phys. Fluids 16, L55-L58 (2004).
- ¹⁹G. McHale, M. I. Newton, and N. J. Shirtcliffe, "Immersed superhydrophobic surfaces: Gas exchange, slip and drag reduction properties," Soft Matter 6, 714-
- 20 M. Castagna, N. Mazellier, and A. Kourta, "Wake of super-hydrophobic falling spheres: Influence of the air layer deformation," J. Fluid Mech. 850, 646-673
- ²¹J. W. Gose, K. Golovin, M. Boban, J. M. Mabry, A. Tuteja, M. Perlin, and S. L. Ceccio, "Characterization of superhydrophobic surfaces for drag reduction in turbulent flow," J. Fluid Mech. 845, 560-580 (2018).
- ²²R. A. Bidkar, L. Leblanc, A. J. Kulkarni, V. Bahadur, S. L. Ceccio, and M. Perlin, "Skin-friction drag reduction in the turbulent regime using random-textured hydrophobic surfaces," Phys. Fluids 26, 085108 (2014).
- ²³K. Alamé and K. Mahesh, "Wall-bounded flow over a realistically rough superhydrophobic surface," J. Fluid Mech. 873, 977-1019 (2019).
- 24A. Busse and N. D. Sandham, "Influence of an anisotropic slip-length boundary condition on turbulent channel flow," Phys. Fluids 24, 055111 (2012).
- 25W. A. Rowin and S. Ghaemi, "Streamwise and spanwise slip over a superhydro-
- phobic surface," J. Fluid Mech. 870, 1127-1157 (2019).

 ²⁶A. Rastegari and R. Akhavan, "On drag reduction scaling and sustainability bounds of superhydrophobic surfaces in high Reynolds number turbulent flows," J. Fluid Mech. 864, 327-347 (2019).
- ²⁷D. G. Crowdy, "Slip length formulas for longitudinal shear flow over a superhydrophobic grating with partially filled cavities," J. Fluid Mech. 925, R2 (2021).
- ²⁸H. Ling, J. Katz, M. Fu, and M. Hultmark, "Effect of Reynolds number and saturation level on gas diffusion in and out of a superhydrophobic surface," Phys. Rev. Fluids 2, 124005 (2017).
- ²⁹L. Zhang, C. R. Crick, and R. J. Poole, "In situ monitor of superhydrophobic surface degradation to predict its drag reduction in turbulent flow," Appl. Phys. Lett. 123, 064101 (2023).
- 30 H. Li, Z. Li, X. Tan, X. Wang, S. Huang, Y. Xiang, P. Lv, and H. Duan, "Threedimensional backflow at liquid-gas interface induced by surfactant," J. Fluid
- $^{\bf 31}{\rm H.}$ Rodriguez-Broadbent and D. G. Crowdy, "Superhydrophobic surfaces with recirculating interfacial flow due to surfactants are 'effectively' immobilized," Fluid Mech. 956, R3 (2023).
- 32 E. Aljallis, M. A. Sarshar, R. Datla, V. Sikka, A. Jones, and C. H. Choi, "Experimental study of skin friction drag reduction on superhydrophobic flat plates in high Reynolds number boundary layer flow," Phys. Fluids 25, 025103 (2013).
- 33C. Lee and C. J. Kim, "Maximizing the giant liquid slip on superhydrophobic microstructures by nanostructuring their sidewalls," Langmuir 25, 12812-12818 (2009).
- 34N. Yu, A. McClelland, F. J. del Campo Melchor, S. Y. Lee, and J. H. Lee, "Sustainability of the plastron on nano-grass-covered micro-trench superhydrophobic surfaces in high-speed flows of open water," J. Fluid Mech. 962, A9
- $^{35}\mathrm{M}.$ Xu, N. Yu, J. Kim, and C. J. C. Kim, "Superhydrophobic drag reduction in high-speed towing tank," J. Fluid Mech. 908, A6 (2020).
- 36 M. Xu, A. Grabowski, N. Yu, G. Kerezyte, J. W. Lee, B. R. Pfeifer, and C. J. Kim, "Superhydrophobic drag reduction for turbulent flows in open water," Phys. Rev. Appl. 13, 034056 (2020).
- ³⁷P. Du, J. Wen, Z. Zhang, D. Song, A. Ouahsine, and H. Hu, "Maintenance of air layer and drag reduction on superhydrophobic surface," Ocean Eng. 130, 328-335 (2017).
- ³⁸J. Breveleri, S. Mohammadshahi, T. Dunigan, and H. Ling, "Plastron restoration for underwater superhydrophobic surface by porous material and gas injection," Colloids Surf. A 676, 132319 (2023).
- ³⁹B. P. Lloyd, P. N. Bartlett, and R. J. K. Wood, "Active gas replenishment and sensing of the wetting state in a submerged superhydrophobic surface," Soft Matter 13, 1413–1419 (2017).
- ⁴⁰D. Panchanathan, A. Rajappan, K. K. Varanasi, and G. H. McKinley, "Plastron regeneration on submerged superhydrophobic surfaces using in situ gas

- generation by chemical reaction," ACS Appl. Mater. Interfaces 10, 33684-33692 (2018).
- ⁴¹S. Hoshian, V. Jokinen, and S. Franssila, "Robust hybrid elastomer/metal-oxide superhydrophobic surfaces," Soft Matter 12, 6526–6535 (2016).
- ⁴²L. Li, J. Zhu, S. Zhi, E. Liu, G. Wang, Z. Zeng, W. Zhao, and Q. Xue, "Study of adhesion and friction drag on a rough hydrophobic surface: Sandblasted aluminum," Phys. Fluids 30, 071903 (2018).
- ⁴³R. Sun, J. Zhao, Z. Li, J. Mo, Y. Pan, and D. Luo, "Preparation of mechanically durable superhydrophobic aluminum surface by sandblasting and chemical modification," Prog. Org. Coat. 133, 77–84 (2019).
- ⁴⁴Z. Zhang, Z. Shen, H. Wu, L. Li, and X. Fu, "Study on preparation of superhydrophobic Ni-Co coating and corrosion resistance by sandblasting–electrodeposition," Coatings 10, 1164–1116 (2020).
- 45 D. Reholon and S. Ghaemi, "Plastron morphology and drag of a superhydrophobic surface in turbulent regime," Phys. Rev. Fluids 3, 104003 (2018).
 46 A. Rajappan, K. Golovin, B. Tobelmann, V. Pillutla, Abhijeet, A. Tuteja, and G.
- ⁴⁶A. Rajappan, K. Golovin, B. Tobelmann, V. Pillutla, Abhijeet, A. Tuteja, and G. H. McKinley, "Influence of textural statistics on drag reduction by scalable, randomly rough superhydrophobic surfaces in turbulent flow," Phys. Fluids 31, 042107 (2019).
- ⁴⁷W. Abu Rowin and S. Ghaemi, "Effect of Reynolds number on turbulent channel flow over a superhydrophobic surface," Phys. Fluids 32, 075105 (2020).
- ⁴⁸A. Rajappan and G. H. McKinley, "Cooperative drag reduction in turbulent flows using polymer additives and superhydrophobic walls," Phys. Rev. Fluids 5, 114601 (2020).
- ⁴⁹J. Seo and A. Mani, "Effect of texture randomization on the slip and interfacial robustness in turbulent flows over superhydrophobic surfaces," Phys. Rev. Fluids 3, 044601 (2018).
- ⁵⁰ J. Seo, R. García-Mayoral, and A. Mani, "Pressure fluctuations and interfacial robustness in turbulent flows over superhydrophobic surfaces," J. Fluid Mech. 783, 448–473 (2015).
- ⁵¹E. J. G. Cartagena, I. Arenas, M. Bernardini, and S. Leonardi, "Dependence of the drag over super hydrophobic and liquid infused surfaces on the textured surface and Weber number," Flow Turbul. Combust. 100, 945–960 (2018).
- 52 J. Seo, R. García-Mayoral, and A. Mani, "Turbulent flows over superhydrophobic surfaces: Flow-induced capillary waves, and robustness of air-water interfaces," J. Fluid Mech. 835, 45–85 (2018).
- 53R. Ma, K. Alamé, and K. Mahesh, "Direct numerical simulation of turbulent channel flow over random rough surfaces," J. Fluid Mech. 908, A40 (2020).
- ⁵⁴S. Mohammadshahi, J. Breveleri, and H. Ling, "Fabrication and characterization of super-hydrophobic surfaces based on sandpapers and nano-particle coatings," Colloids Surf. A 666, 131358 (2023).
- 55M. D. Choudhury, S. Das, A. G. Banpurkar, and A. Kulkarni, "Regression analysis of wetting characteristics for different random surface roughness of polydimethylsiloxane using sandpapers," Colloids Surf. A 647, 129038 (2022).
- ⁵⁶ISO 6344-3, Coated Abrasives—Determination and Designation of Grain Size Distribution—Part 3: Microgrit Sizes (ISO, 2021).

- 57See https://www.grainger.com/know-how/equipment/kh-video-sandpaper-gritchart for more information about Sandpaper Grit Charts & Grades.
- 58B. Bhushan and S. Chilamakuri, "Non-Gaussian surface roughness distribution of magnetic media for minimum friction/stiction," J. Appl. Phys. 79, 5794– 5796 (1996).
- 59J. M. Barros, M. P. Schultz, and K. A. Flack, "Measurements of skin-friction of systematically generated surface roughness," Int. J. Heat Fluid Flow 72, 1–7 (2018).
- ⁶⁰K. A. Flack and M. P. Schultz, "Hydraulic characterization of sandpaper roughness," Exp. Fluids 64, 3 (2023).
- ⁶¹R. B. Dean, "Reynolds number dependence of skin friction and other bulk flow variables in two-dimensional rectangular duct flow," J. Fluids Eng. 100, 215 (1978).
- ⁶²E. S. Zanoun, H. Nagib, and F. Durst, "Refined c_f relation for turbulent channels and consequences for high-Re experiments," Fluid Dyn. Res. 41, 021405 (2009).
- ⁶³R. J. Daniello, N. E. Waterhouse, and J. P. Rothstein, "Drag reduction in turbulent flows over superhydrophobic surfaces," Phys. Fluids 21, 085103 (2009).
- 64F. M. White, Viscous Fluid Flow, 2nd ed. (McGraw-Hill Higher Education, 2006)
- 65 M. P. Schultz and K. A. Flack, "The rough-wall turbulent boundary layer from the hydraulically smooth to the fully rough regime," J. Fluid Mech. 580, 381– 405 (2007).
- ⁶⁶L. Joly, C. Ybert, E. Trizac, and L. Bocquet, "Hydrodynamics within the electric double layer on slipping surfaces," Phys. Rev. Lett. 93, 257805 (2004).
- 67P. Joseph and P. Tabeling, "Direct measurement of the apparent slip length," Phys. Rev. E 71, 035303 (2005).
- ⁶⁸K. Fukagata, N. Kasagi, and P. Koumoutsakos, "A theoretical prediction of friction drag reduction in turbulent flow by superhydrophobic surfaces," Phys. Fluids 18, 051703 (2006).
- ⁶⁹J. Seo and A. Mani, "On the scaling of the slip velocity in turbulent flows over superhydrophobic surfaces," Phys. Fluids 28, 025110 (2016).
- ⁷⁰R. Poetes, K. Holtzmann, K. Franze, and U. Steiner, "Metastable underwater superhydrophobicity," Phys. Rev. Lett. 105(1), 166104 (2010).
- 71S. Srinivasan, J. A. Kleingartner, J. B. Gilbert, R. E. Cohen, A. J. B. Milne, and G. H. McKinley, "Sustainable drag reduction in turbulent Taylor-Couette flows by depositing sprayable superhydrophobic surfaces," Phys. Rev. Lett. 114(1), 014501 (2015).
- ⁷²D. Moreira, S. H. Park, S. Lee, N. Verma, and P. R. Bandaru, "Dynamic superhydrophobic behavior in scalable random textured polymeric surfaces," J. Appl. Phys. 119, 125302 (2016).
- ⁷³M. Sakai, A. Nakajima, and A. Fujishima, "Removing an air layer from a superhydrophobic surface in flowing water," Chem. Lett. 39, 482–484 (2010).
- ⁷⁴Q.-S. Zheng, Y. Yu, and Z.-H. Zhao, "Effects of hydraulic pressure on the stability and transition of wetting modes of superhydrophobic surfaces," <u>Langmuir</u> 21, 12207–12212 (2005).